Stem Cell Reports
Article

ISSCR

OPEN ACCESS

In Vitro Models of *GJB2*-Related Hearing Loss Recapitulate Ca^{2+} Transients via a Gap Junction Characteristic of Developing Cochlea

Ichiro Fukunaga,[1,2] Ayumi Fujimoto,[1] Kaori Hatakeyama,[1] Toru Aoki,[1] Atena Nishikawa,[1] Tetsuo Noda,[3,4] Osamu Minowa,[3,4] Nagomi Kurebayashi,[5] Katsuhisa Ikeda,[1] and Kazusaku Kamiya[1,*]

[1]Department of Otorhinolaryngology, Juntendo University Faculty of Medicine, 2-1-1 Hongo, Bunkyo-ku, Tokyo 113-8421, Japan
[2]Research Institute for Diseases of Old Age, Juntendo University Graduate School of Medicine, 2-1-1 Hongo, Bunkyo-ku, Tokyo 113-8421, Japan
[3]Department of Cell Biology, Japanese Foundation for Cancer Research, Cancer Institute, 3-8-31 Ariake, Koto-ku, Tokyo 135-8550, Japan
[4]Team for Advanced Development and Evaluation of Human Disease Models, RIKEN BioResource Center, 3-1-1 Koyadai, Tsukuba, Ibaraki 305-0074, Japan
[5]Department of Cellular and Molecular Pharmacology, Juntendo University Graduate School of Medicine, 2-1-1 Hongo, Bunkyo-ku, Tokyo 113-8421, Japan
*Correspondence: kkamiya@juntendo.ac.jp
http://dx.doi.org/10.1016/j.stemcr.2016.10.005

SUMMARY

Mutation of the Gap Junction Beta 2 gene (*GJB2*) encoding connexin 26 (CX26) is the most frequent cause of hereditary deafness worldwide and accounts for up to 50% of non-syndromic sensorineural hearing loss cases in some populations. Therefore, cochlear CX26-gap junction plaque (GJP)-forming cells such as cochlear supporting cells are thought to be the most important therapeutic target for the treatment of hereditary deafness. The differentiation of pluripotent stem cells into cochlear CX26-GJP-forming cells has not been reported. Here, we detail the development of a novel strategy to differentiate induced pluripotent stem cells into functional CX26-GJP-forming cells that exhibit spontaneous ATP- and hemichannel-mediated Ca^{2+} transients typical of the developing cochlea. Furthermore, these cells from CX26-deficient mice recapitulated the drastic disruption of GJPs, the primary pathology of *GJB2*-related hearing loss. These in vitro models should be useful for establishing inner-ear cell therapies and drug screening that target *GJB2*-related hearing loss.

INTRODUCTION

Hearing loss is the most common congenital sensory deficit (Chan et al., 2010). Approximately 1 child in 1,000 is affected with severe hearing loss at birth or during early childhood, and this is defined as prelingual deafness (Morton, 1991; Petersen and Willems, 2006), with about half of the cases attributable to genetic causes (Birkenhager et al., 2010). There are more than 100 known forms of non-syndromic deafness associated with identified genetic loci (available at http://hereditaryhearingloss.org). Mutations in the Gap Junction Beta 2 gene (*GJB2*), encoding connexin 26 (CX26), account for up to 50% of cases of non-syndromic sensorineural hearing loss in some populations (Morton and Nance, 2006). CX26 and CX30, which are encoded by *GJB6*, co-assemble and participate in the formation of gap junctions between cells, and these connexins are the two most abundantly expressed gap junction proteins in the cochlea (Ahmad et al., 2003) (Figure S1 and Movie S1).

Gap junctions facilitate the rapid removal of K^+ from the base of the cochlear hair cells, resulting in K^+ recycling back to the endolymph to maintain cochlear homeostasis (Kikuchi et al., 2000). CX26 is also involved in the developmental organization of mammalian cochlea, for example, tunnel of Corti, Nuel's space, or spaces surrounding the outer hair cells (Inoshita et al., 2008). CX26 and CX30 form heteromeric and heterotypic channels in most of the cochlear gap junction plaques (GJPs) (Sun et al., 2005) and in in vitro experiments (Yum et al., 2007). Recently, expression of various transcription factors and other proteins in human developmental fetal cochleae from gestational weeks 9–22 were investigated using immunohistochemistry (Locher et al., 2013, 2014), and it has been found that the expression of CX26 and CX30 is detectable in the outer sulcus cells at 18 weeks of gestation (Locher et al., 2015).

In our recent study, it was shown that disruption of the CX26 GJP is associated with the pathogenesis of *GJB2*-related hearing loss and that the assembly of cochlear GJP is dependent on CX26 (Kamiya et al., 2014). It was also reported that cochlear gene transfer of *GJB2* using an adeno-associated virus significantly improved GJP formation and auditory function (Iizuka et al., 2015). In our alternative approach, a novel strategy was developed for inner-ear cell therapy with bone marrow mesenchymal stem cells (Kamiya et al., 2007).

Induced pluripotent stem cells (iPSCs) can be produced by the reprogramming of somatic cells, and are capable of self-renewal and differentiation into various types of cells such as embryonic stem cells (ESCs) (Takahashi and Yamanaka, 2006). Human cochlear cells are not readily accessible for biopsy or direct drug administration because of anatomical limitations. Therefore, ESCs/iPSCs are an important tool for studying the molecular mechanisms underlying inner-ear pathology as well as for generating cells for replacement therapies. It was recently reported that ESCs/iPSCs could be differentiated into inner-ear progenitor cells by in vitro differentiation in adherent monolayer culture and/or floating aggregation culture

(Chen et al., 2012; Koehler and Hashino, 2014; Koehler et al., 2013; Oshima et al., 2010). For recapitulation of neural tissue formation in a three-dimensional (3D) context, floating aggregation culture is advantageous as it allows more flexible adaptation of cell and tissue shapes compared with 2D culture approaches (Eiraku and Sasai, 2012). Eiraku et al. (2011) reported in vitro differentiation of ESCs into cortical tissues when the cells were cultured as floating aggregates in a serum-free medium, thereby establishing the technique of serum-free floating culture of embryoid body-like aggregates with quick re-aggregation (SFEBq culture). Koehler and colleagues reported differentiation of ESCs into inner-ear hair cell-like cells using modified SFEBq methods (Koehler and Hashino, 2014; Koehler et al., 2013). For the establishment of strategies for inner-ear cell therapy or the development of a disease model for *GJB2*-related hearing loss, it is necessary to develop efficient differentiation methods for inducing iPSCs to form cells with CX26-containing GJPs. Although several studies have demonstrated the induced differentiation of ESCs/iPSCs into CX37/40/43/45-expressing cells (Mauritz et al., 2008; Oyamada et al., 1996, 2013), no such protocol has been reported for the differentiation of ESCs/iPSCs into CX26-expressing cells.

Here we developed an efficient induction method for the differentiation of mouse iPSCs into CX26-expressing cells that, through subsequent adherent culture on cochlear feeder cells, form CX26-GJPs typical of cochlear tissue.

RESULTS

Non-neural Ectoderm Induction in Three-Dimensional Culture and Screening of High-CX26/CX30 Aggregates

To develop disease model cells targeting *GJB2*-related hearing loss, we induced CX26-expressing GJP-forming cells from iPSCs using methods modified from previous studies for the differentiation of inner-ear sensory epithelia (Koehler and Hashino, 2014; Koehler et al., 2013). On day 7 of differentiation, aggregates showed similar morphology composed of differentiated outer regions and undifferentiated core regions (NANOG-GFP-positive cells, Figure S2) as previously reported (Koehler and Hashino, 2014; Koehler et al., 2013). In this study, we used the NANOG-GFP reporter system to monitor the differentiation level. *NANOG* is a transcription factor used to identify undifferentiated cells. To screen the conditions to induce high CX26/CX30 expression, we compared mRNA levels in day-7 aggregates, including addition of bone morphogenetic protein 4 (BMP-4: BMP), inhibitor of activating receptor-like kinase (ALK) receptors (SB-431542: SB), BMP/SB (B/S), B/S + fibroblast growth factor 2 (FGF-2: B/S + FGF), B/S + inhibitor of ALK receptors (LDN-193189: B/S + LDN), and B/S + FGF/LDN (B/S + F/L) (Figure 1A). CX26/CX30 levels were significantly higher especially in BMP and B/S. In contrast to B/S + F/L, a condition for hair cell differentiation (Koehler and Hashino, 2014; Koehler et al., 2013), BMP and B/S showed high mRNA levels both for CX26 and CX30. Therefore, these two conditions were selected for further isolation of CX26/CX30-expressing cells. On days 7–11 of differentiation, BMP- and B/S-treated aggregate were transferred to adherence culture (2D) with trypsin-resistant inner-ear cells (TRIC), which we generated as feeder cells (see Experimental Procedures) (Figure 1B).

CX26-GJP-Forming Cells in iPSC-Derived Aggregate

To analyze the localization of CX26 in iPSC aggregates, we performed immunohistochemistry with day-7 aggregates for which BMP and B/S showed the highest CX26/CX30 mRNA increases (Figure 1A). These aggregates formed a distinct outer epithelium that enclosed small vesicles (Figures 1C and 1D). In a number of cells and particularly within these vesicles, we distinguished large planar CX26-containing GJPs, which, as we reported previously (Kamiya et al., 2014), are characteristic of normal mouse cochlea (Figures 1E–1H, S3D, and S3E). These cells, termed iPSC-derived CX26-expressing GJP-forming cells (iCx26GJCs), were disseminated throughout the small vesicles of the aggregates. In contrast, undifferentiated (Nanog-positive) iPSCs and TRIC feeder cells did not show immunolabeling for CX26 (Figures S3A–S3C). We also used scanning electron microscopy (EM) to examine the ultrastructure of cell surfaces and borders of the small vesicles from BMP/SB-treated aggregates. The surfaces of the small vesicles showed distinct cell borders with associated microvilli (Figures 1I–1K).

The iCx26GJC in 2D Cultures Formed CX26-Containing GJPs as in the Developing Cochlea

The regions with iCx26GJC-containing small vesicles were separated from day 7–11 aggregates and subcultured in growth medium on TRIC feeder cells (Figure 1B). With other feeder cells, for example, feeder cells from chicken embryonic inner ear, or in non-feeder conditions on non-coated or gelatin-coated dishes, the separated outer epithelia and small vesicles did not proliferate and were effectively dead. Although the iPSC aggregates that had been subcultured on Matrigel-coated dishes proliferated, CX26 was not observed by immunohistochemistry (data not shown). We observed migration and proliferation of subcultured small vesicles in 2D culture (Movie S2). The subcultured small vesicles indeed colonized on TRIC feeder cells, and the colonies contained iCx26GJC. In TRIC feeder cells, iCx26GJCs proliferated significantly in adherent culture conditions, and the CX26-containing GJPs were

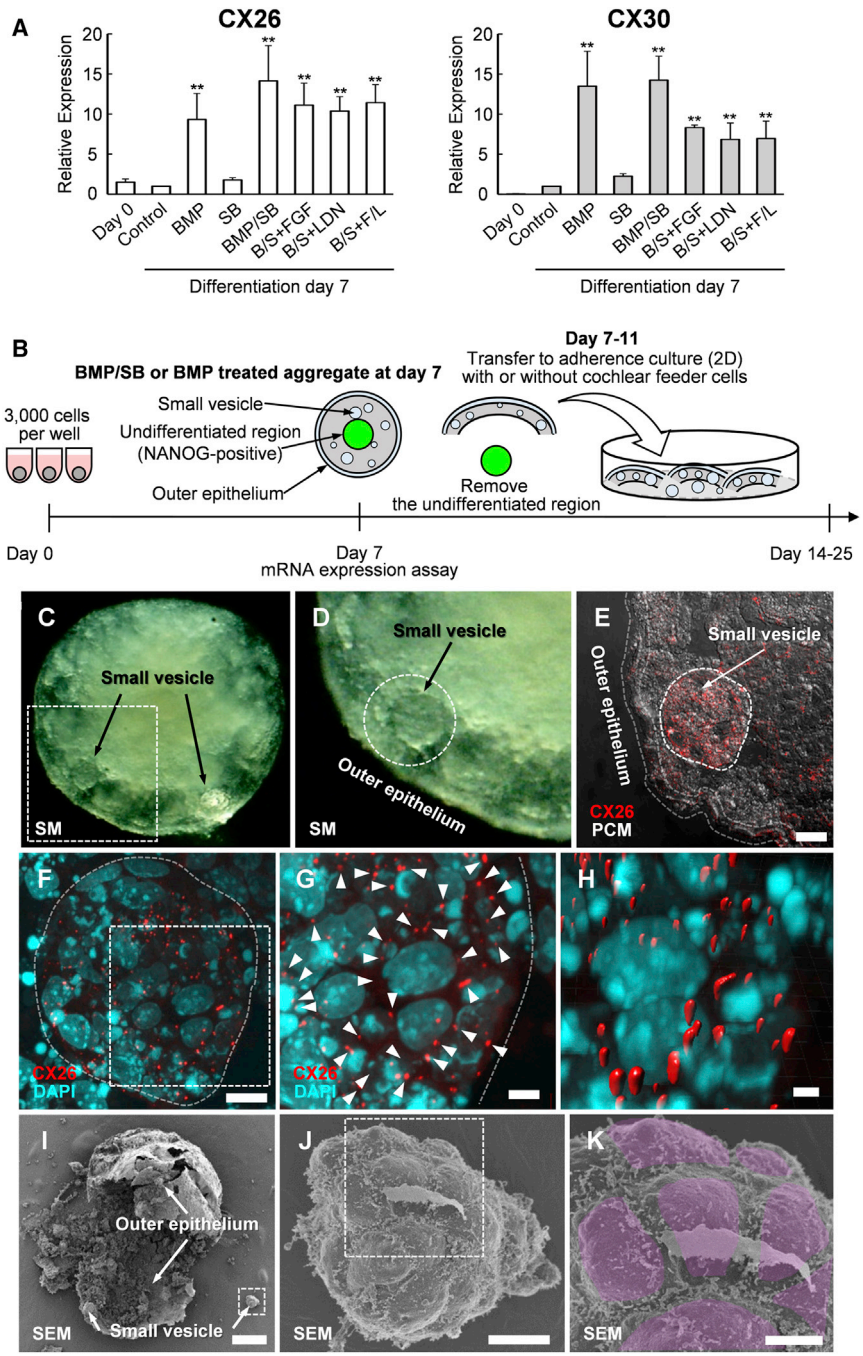

Figure 1. The Inner-Ear Induction of iPSC-Derived Aggregates Based on CX26/CX30 Expression

(A) qPCR analysis of mRNA to assay effects of growth factor/inhibitor addition on day-0 (undifferentiated iPSCs) and day-7 aggregates. mRNA expression levels were calculated relative to untreated aggregates (control). BMP, human bone morphogenetic protein 4; SB, SB-431542, inhibitor of activin receptor-like kinase (ALK) receptors; FGF, human fibroblast growth factor 2; LDN, LDN-193189, inhibitor of ALK receptors; F/L, the combination of FGF and LDN. Both CX26 and CX30 were significantly upregulated in BMP, BMP/SB, B/S+FGF, B/S+LDN, and B/S/+F/L samples compared with controls. Statistical differences were determined by Student's t test. n = 4 independent experiments, mean ± SE; **p < 0.01.

(B) Inner-ear induction strategy.

(C) Stereo microscopic image of the BMP/SB-treated aggregates at day 7.

(D) Magnification of boxed region in (C). The small vesicle is encircled by a dashed line.

(E) Merge of CX26 (red) and phase contrast microscopy (PCM; white) images in the cryosection. A small vesicle is encircled by a dashed line.

(F) Merge of CX26 (red) and DAPI (blue) images. Magnification of the small vesicle in (E).

(G) Magnification of boxed region in (F). Arrowheads point to GJPs.

(H) The 3D image was reconstructed from the image in (G).

(I) Scanning EM shows the undifferentiated region, outer epithelium, and small vesicles.

(J) Magnification of boxed region in (I).

(K) Magnification of boxed region in (J). Surface of the small vesicle. The individual cells, which form the surface of the small vesicle, are colored.

Scale bars represent 100 μm (I), 20 μm (E), 10 μm (F and J), 5 μm (G and K), and 2 μm (H).

preserved (Figures 2E–2H and Movie S3) as in the cochlear supporting cells—specifically the outer- and inner-sulcus cells (Figures 2A–2C). Although the proportion of iCx26GJCs was only 1.8% ± 1.0% and 1.8% ± 1.0% in the aggregates of BMP and B/S, respectively, they increased to 32.2% ± 7.4% and 45.1% ± 9.6% in the 2D culture on TRIC feeder cells (Figure 2I). Lengths of the largest GJPs along a single cell border were 2.46 ± 0.45 μm and 1.86 ± 0.15 μm in the BMP- or B/S-treated aggregates, respectively, and were significantly increased to 4.02 ± 0.2 μm and 5.76 ± 0.35 μm in the 2D culture on TRIC feeder cells (Figure 2J).

The iCx26GJCs Co-expressed CX30, P27^{kip1}, and SOX2

To examine the similarities to cochlear cells, we analyzed the expression of known cochlear proteins using immunohistochemistry. CX30 protein, another causative gene

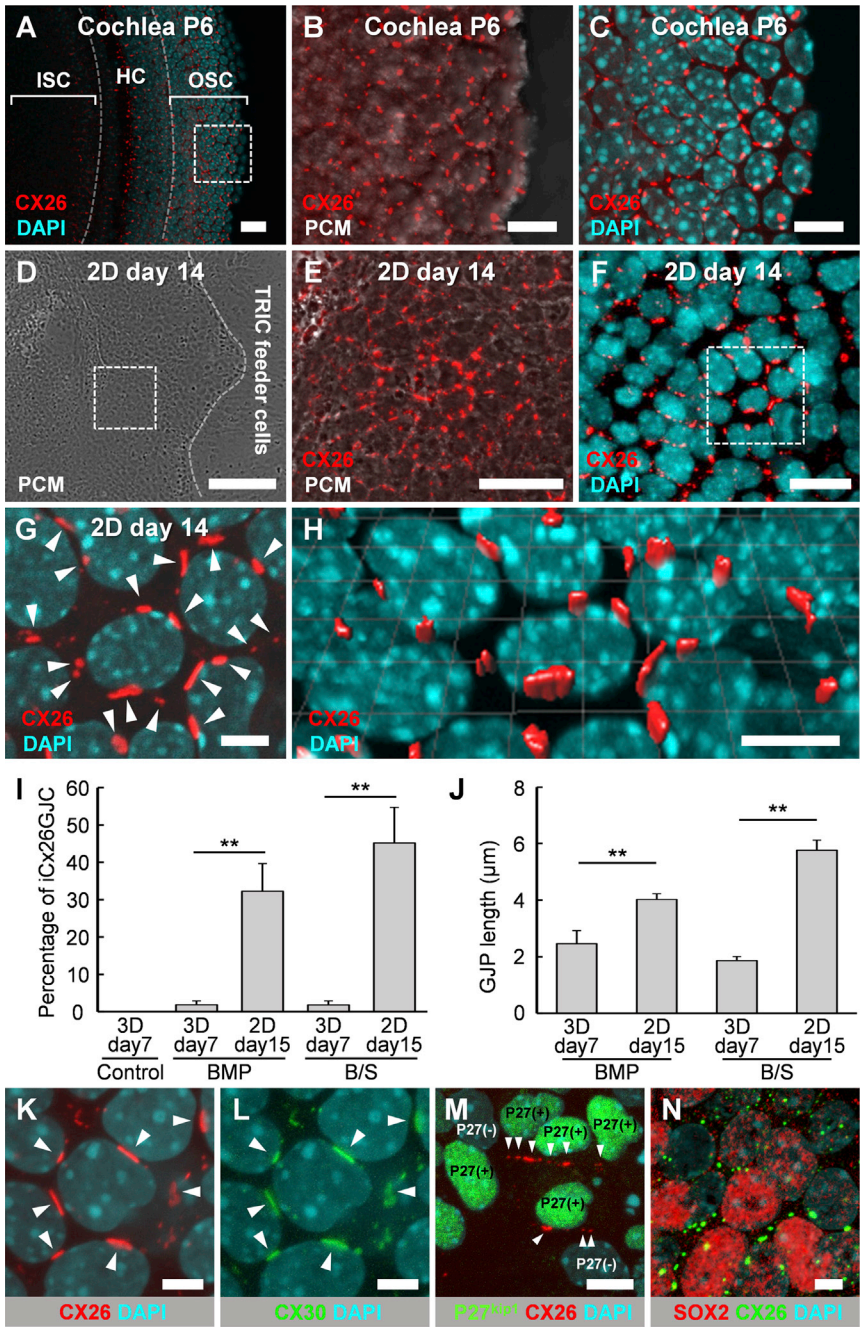

Figure 2. Immunohistological Analysis in Mouse Cochlea and 2D Culture

(A) CX26 (red) expression in P6 mouse cochlea. Nuclei were stained by DAPI (blue). ISC, inner-sulcus cells; OSC, outer sulcus cells; HC, hair cells.

(B) Magnification of boxed region in (A). Merge of CX26 (red) and PCM (white) images.

(C) Magnification of boxed region in (A).

(D) PCM images in 2D culture at day 14.

(E) Magnification of boxed region in (D). Merge of CX26 (red) and PCM (white) images.

(F) Staining for CX26 (red) and DAPI (blue).

(G) Magnification of boxed region in (F). Arrowheads point to GJPs.

(H) The 3D image was reconstructed from the image in (G).

(I) Percentage of iCx26GJC in 3D culture at day 7 and 2D culture on TRIC at day 15 (3D culture: n = 15 from three independent experiments; 2D culture: n = 20 from four independent experiments). The statistical difference was determined by Student's t test, mean ± SE; $^{**}p < 0.01$.

(J) Lengths of the largest GJPs along a single cell border in 3D culture at day 7 and 2D culture at day 15 (3D culture: n = 5 from three independent experiments; 2D culture: n = 25 from five independent experiments). The statistical difference was determined by Student's t test, mean ± SE; $^{**}p < 0.01$.

(K) Staining for CX26 (red) and DAPI (blue) in 2D culture at day 14. Magnification of boxed region in Figure S4E. Arrowheads point to GJPs.

(L) Staining for CX30 (green) and DAPI (blue) in 2D culture at day 14. Magnification of boxed region in Figure S4E. Arrowheads point to GJPs.

(M) Staining for CX26 (red), $P27^{kip1}$ (green), and DAPI (blue) in 2D culture at day 15. Heterogeneous $P27^{kip1}$-positive regions including iCx26GJCs. Magnification of boxed region in Figure S5E. Arrowheads point to GJPs.

(N) Staining for SOX2 (red), CX26, and DAPI (blue) in 2D culture at day 15. Heterogeneous SOX2-positive regions including iCx26GJCs. Magnification of boxed region in Figures S6D–S6F.

Scale bars represent 200 μm (D), 50 μm (A and E), 10 μm (B, C, F, and H), and 5 μm (G and K–N).

product frequently encountered in hereditary deafness, co-localized with CX26 in most of the CX26-GJPs of the differentiated cells (Figures 2K, 2L, and S4E–S4H). Therefore, we inferred that CX26 and CX30 were the two main components of these GJPs, as was the case in the cochlear supporting cells—specifically the outer- and inner-sulcus cells (Figures S4A–S4D). Furthermore, the iCx26GJCs on TRIC feeder cells co-expressed $P27^{kip1}$ (Figures 2M and S5C–S5I), which is a cyclin-dependent kinase inhibitor expressed in cochlear supporting cells such as the Deiters' cells and outer- and inner-sulcus cells (Figures S5A and S5B). The $P27^{Kip1}$ signals were observed after day

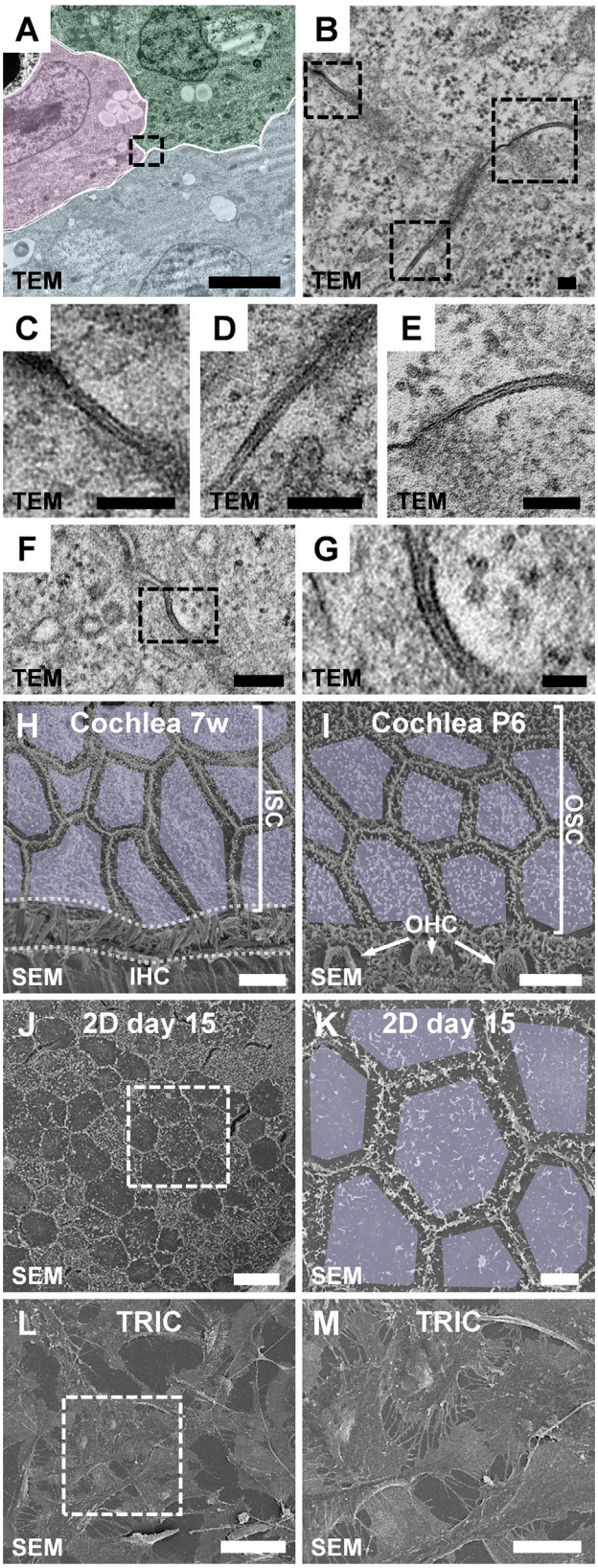

Figure 3. Ultrastructure of Gap Junctions in iPSC-Derived Aggregates at Day 7, Cell Surfaces in Cochlea, 2D Cultures at Day 15, and TRIC Feeder Cells

(A) TEM of tricellular junction (green, pink, blue) in BMP-treated aggregates at day 7.

(B) Magnification of boxed region in (A). Ultrastructure corresponding to three gap junctions was observed at the tricellular junction.

(C–E) Magnification of boxed regions in (B).

(F) TEM of gap junction in BMP/SB-treated aggregate at day 7.

(G) Magnification of boxed region in (F). Ultrastructure is typical of gap junctions, with clear distinct intermembrane layer between the plasma membranes.

(H) Scanning EM of cell surfaces and borders in cochlea from a 7-week-old mouse. The individual cells are colored. ISC, inner-sulcus cell; IHC, inner hair cell.

(I) Scanning EM of cell surfaces and borders in cochlea from a P6 mouse. The individual cells are colored. OSC, outer sulcus cell; OHC, outer hair cell.

(J) Scanning EM of cell surfaces and borders in 2D culture at day 15.

(K) Magnification of boxed region in (J). The surface and borders of cells from 2D culture were quite similar to those of cochlear cells. The individual cells are colored.

(L) Scanning EM of cell surfaces and borders in TRIC feeder cells.

(M) Magnification of boxed region in (L).

Scale bars represent 50 μm (L), 20 μm (J and M), 10 μm (H), 5 μm (A, I, and K), 200 nm (F), 100 nm (B–E), and 50 nm (G).

15, corresponding to the stage at which the colony expansion (Movie S2) had almost stopped (~days 14–16). We observed both heterogeneous (Figures 2M and S5C–S5E) and homogeneous (Figures S5F–S5I) $P27^{Kip1}$-positive regions including iCx26GJCs under the same condition. Furthermore, SOX2, which is a transcript factor essential for maintaining self-renewal, or pluripotency, of undifferentiated or neural stem cells, was co-expressed in part of cochlear supporting cells (Figures S6A–S6C). SOX2 signals were partly observed in iCx26GJCs at day 15. We observed both $CX26^{+}/SOX2^{+}$ cells and $CX26^{+}/SOX2^{-}$ cells in the same cell population (Figures 2N and S6D–S6I).

Ultrastructure of Gap Junctions and Cell Surfaces in iPS-Derived Cells

We also analyzed the ultrastructure at the cell junction sites in transmission electron micrographs (TEM) of iPSC-derived aggregates. We found ultrastructure typical of gap junctions, i.e., an intercellular layer between the two distinct plasma membranes with a uniform intermembrane space of ~2–4 nm (Figures 3A–3G). Figures 3C–3E show three distinct gap junctions around a tricellular junction site among three iPS-derived cells. Such characteristic ultrastructures of gap junctions were observed in two medium conditions, BMP (Figures 3A–3E) and B/S (Figures 3F and 3G), but not in the others (data not shown).

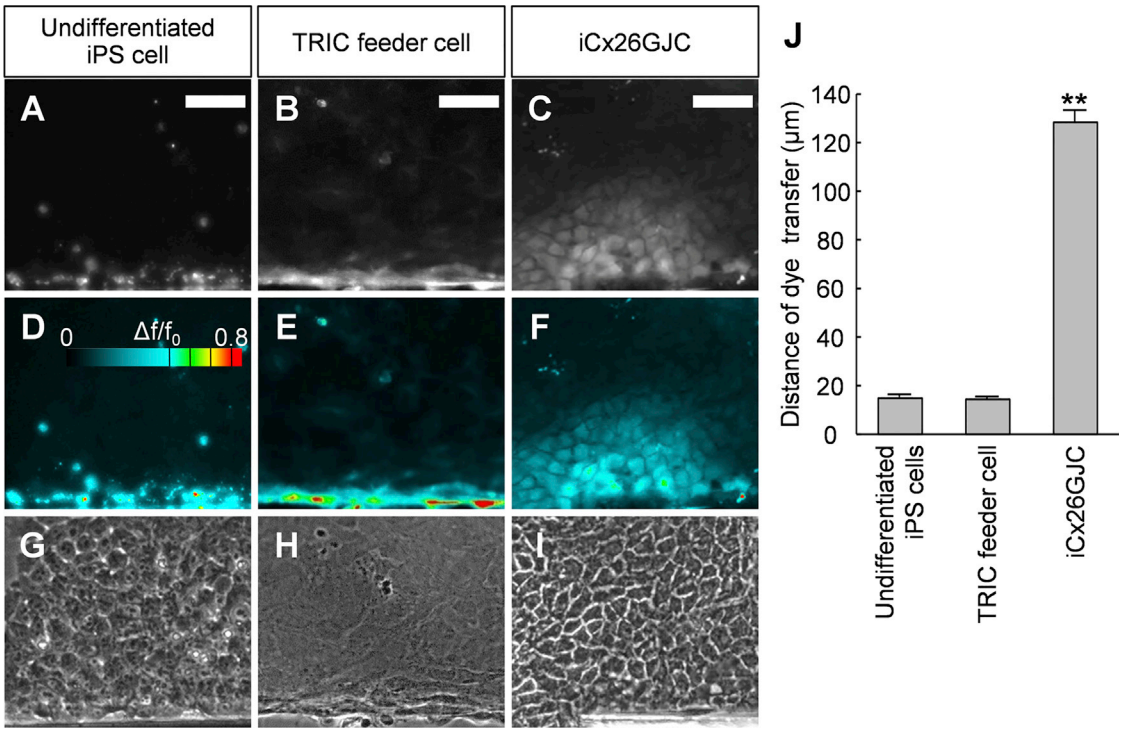

Figure 4. Dye Transfer after Scrape-Loading Cells and Quantitative Analysis

Digital fluorescence images of cultured cells after scrape loading. The undifferentiated iPSCs (A, D, and G), TRIC feeder cells (B, E, and H) and BMP/SB-treated iPSC-derived 2D culture containing iCx26GJC at day 15 (C, F, and I) were incubated in 0.1% LY and imaged 15 min after wounding with a scalpel blade. Wounded cells integrated dye in all cases, but there was no transfer of dye from primary wounded cells to neighboring cells.

(A–C) Dye transfer using LY.

(D–F) Pseudocolor images indicating the range from low (black) to high (red) signal intensity of the images in (A)–(C), respectively.

(G–I) Phase contrast microscopy.

(J) Quantitative analysis of intercellular LY transfer after scrape loading. Columns represent the mean distance of LY transfer from the scrape line to the point where the fluorescence intensity dropped to 1.5× the background intensity (TRIC feeder cells and undifferentiated iPSCs: n = 20 from four independent experiments; iCx26GJC: n = 68 from six independent experiments). The statistical difference was determined by Scheffe's multiple comparison test, mean ± SE; **$p < 0.01$.

Scale bars represent 50 μm.

We also examined the ultrastructure of the cell surfaces and borders using scanning EM of 2D cultures at day 15 (Figures 3J and 3K). The cell surfaces of 2D culture showed distinct, straight cell borders that formed hexagonal or pentagonal shapes with microvilli distributed along the borders as in normal cochlea (Figures 3H and 3I). In contrast, TRIC feeder cells showed unstructured cell borders without microvilli as in conventional mesenchymal cells (Figures 3L and 3M).

Functional Gap Junction Intercellular Communication Networks in iCx26GJCs

To investigate whether the gap junction structures observed in proliferated iCx26GJCs (Figures 2 and 3) were functional in the formation of gap junction intercellular communication (GJIC) networks, we performed scrape-loading assays with Lucifer yellow (LY) (Yum et al., 2007) on proliferated iCx26GJCs, with undifferentiated iPSCs and TRIC feeder cell as controls. We used two different iPSC strains and repeated the experiments at least three times, with similar results. We quantified the extent of dye transfer by measuring the distance from the scrape line to the point where the fluorescence intensity dropped to 1.5× the background fluorescence intensity. In the iCx26GJC culture, we observed that LY diffused beyond the wounded parental cells (Figures 4C and 4F). In contrast, such extent of dye transfer was not observed in undifferentiated iPSCs or cochlear feeder cells (Figures 4A, 4B, 4D, and 4E). As shown in the Figure 4J, quantitative distance of dye transfer in iCx26GJCs (128.2 ± 4.24 μm) was significantly longer ($p < 0.01$) than in undifferentiated iPSCs (14.8 ± 0.96 μm) or TRIC feeder cells (14.3 ± 0.74 μm).

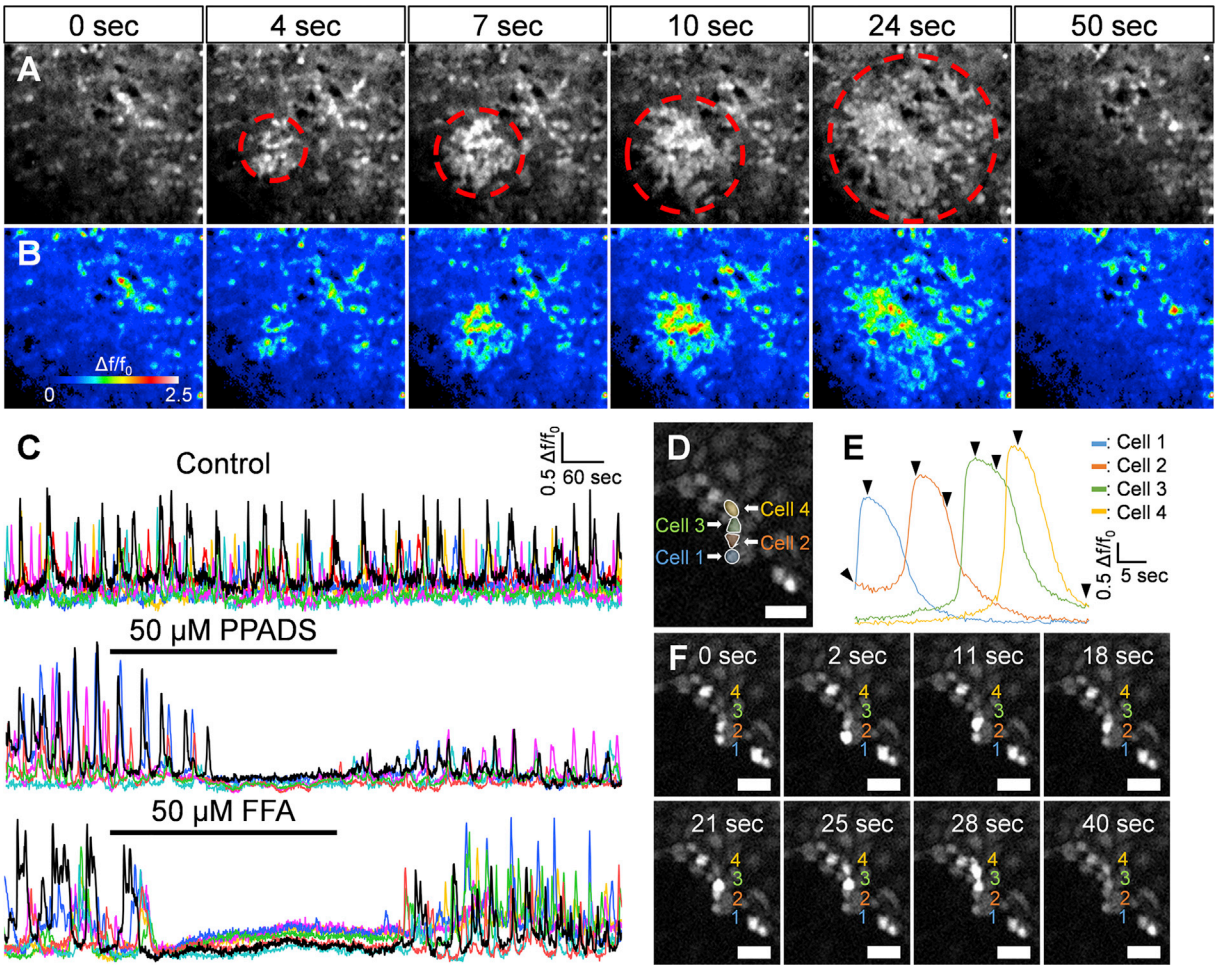

Figure 5. Propagation of Spontaneous Ca^{2+} Transients in 2D Culture

(A) The propagation of spontaneous Ca^{2+} transients at each time point (0, 4, 7, 10, 24, and 50 s) at near-physiological temperature (32°–35°C). The propagation region is encircled by a dashed red line.

(B) Pseudocolor images indicating the range from low (black) to high (white) signal intensity of the images in (A). The cells were imaged for 50 s at one frame per 500 ms.

(C) Spontaneous Ca^{2+} signaling activity is reversibly inhibited by the p2x receptor antagonist PPADS and the connexin hemichannel blocker FFA (flufenamic acid). The cells were imaged for 14 min at one frame per 500 ms.

(D) Regions of interest in 2D cultures at 22°–24°C with longer intercellular Ca^{2+} signal intervals.

(E) Time-dependent changes in fluorescence intensity in four cells (labeled 1–4). Cells were imaged for 40 s at one frame per 260 ms. Arrowheads indicate time points corresponding to those in (F).

(F) Fluorescence intensity in four cells at each time point (0, 2, 11, 18, 21, 25, 28, and 40 s).

Scale bars represent 20 μm.

Propagation of Spontaneous Ca^{2+} Transients via Gap Junctions in iCx26GJCs

To test whether iCx26GJCs propagate spontaneous Ca^{2+} transients via gap junctions in the developing auditory system (Anselmi et al., 2008; Tritsch et al., 2007), we performed Ca^{2+} imaging with the Ca^{2+} indicator fluo-4. Spontaneous Ca^{2+} transients and their propagation were detected in 2D cultures under the B/S condition (Figures 5A, 5B, and 5D–5F; Movies S4 and S6). The BMP condition also showed the same Ca^{2+} transients and propagation (data not shown), although the frequency was much less than under the B/S condition.

Ca^{2+} Activity in iCx26GJCs Required ATP and Hemichannels as in Developing Cochlea

To investigate whether this spontaneous Ca^{2+} activity required ATP and hemichannels, as reported for this activity in developing cochlea (Schutz et al., 2010; Tritsch et al.,

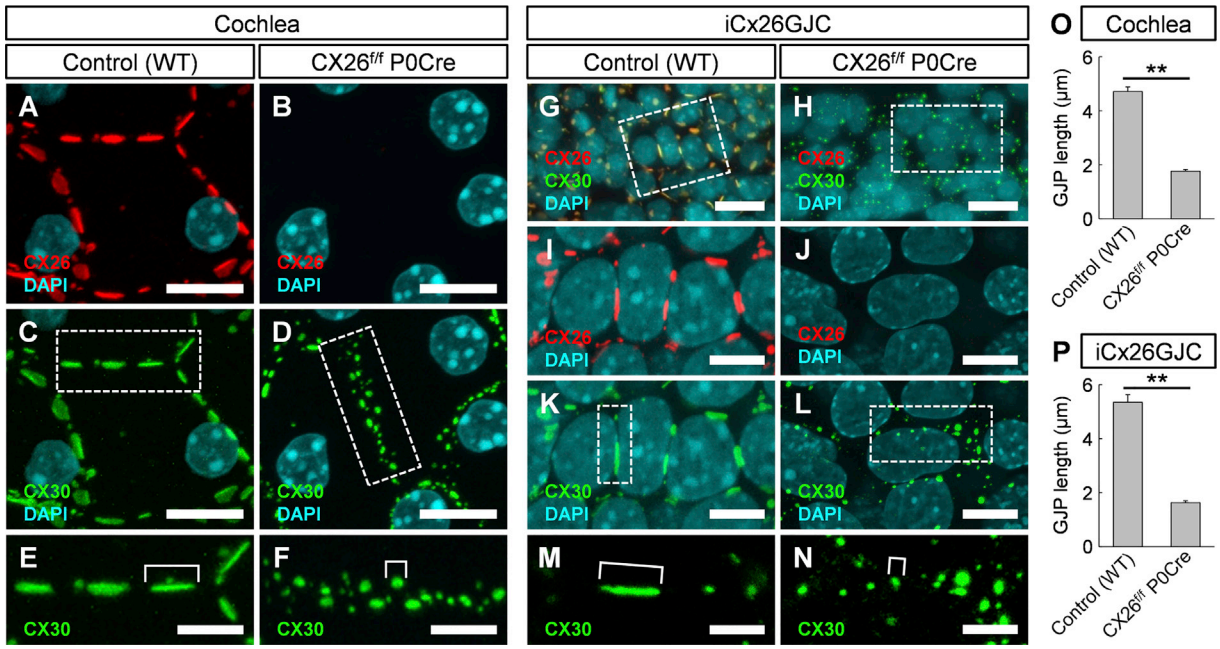

Figure 6. The iCx26GJCs from CX26-Deficient Mouse Recapitulated the Drastic Disruption of GJPs as in Cochlea

(A–N) GJP formation in 16-week-old adult mouse cochleae (A–F) and iCx26GJC at day 15 (G–N). These samples were co-labeled with anti-CX26 (red) and anti-CX30 (green) antibodies and were counterstained with DAPI (blue). WT-iCx26GJC showed large, planar GJPs (G, I, K, and M) as WT mouse cochlea (A, C, and E). In contrast, $CX26^{f/f}$ P0-Cre-iCx26GJC showed drastically fragmented, small vesicle-like GJPs (H, J, L, and N) as $CX26^{f/f}$ P0-Cre-mouse cochlea (B, D, and F). (I and J) Image of each boxed region in (G) and (H), respectively. (E, F, M, and N) Image of each boxed region in (C), (D), (K), and (L), respectively.

(O and P) Length of the largest GJPs (brackets in E, F, M, and N) along a single cell border (mean ± SE, n = 25, 38, 41, 48 cell borders from four independent experiments). The statistical difference was determined by Student's t test; $^{**}p < 0.01$.

Scale bars represent 20 μm (G and H), 10 μm (A–D and I–L), and 5 μm (E, F, M, and N).

2007), we pharmacologically inhibited Ca^{2+} activity with the p2x receptor antagonist PPADS (pyridoxal-phosphate-6-azophenyl-2′,4′-disulphonic acid) (Tritsch et al., 2007) and connexin hemichannel blocker FFA (flufenamic acid) (Anselmi et al., 2008; Bruzzone et al., 2005; Eskandari et al., 2002; Gomes et al., 2005; Schutz et al., 2010; Stout et al., 2002; Zhang et al., 1998). The spontaneous Ca^{2+} signaling activity was clearly inhibited by PPADS and FFA, and the activity was restored after removal of the inhibitors (Figure 5C and Movie S5). In these analysis, subset of the cells showed continuous slow oscillation at random regions of the cell culture (Movie S5) and some of them showed clear propagated waves as in developing cochlea (Figures 5A, 5B, and 5D–5F; Movies S4 and S6).

iCx26GJC Derived from CX26-Deficient Deafness Mouse Recapitulated GJP Disruption as in the Cochlea

To investigate whether the induction strategy can apply to disease model for CX26-associated deafness, we generated an iPSC line from a CX26-deficient deafness mouse model, $CX26^{f/f}$ P0-Cre (Kamiya et al., 2014), and tested the potential of this iPSC line to differentiate into GJP-forming cells. WT-iCx26GJC showed large, planar GJPs (Figures 6G, 6I, 6K, and 6M) at the cell border that formed an orderly pentagonal structure of hexagonal outlines, as in the wild-type (WT) cochlea. In contrast, $CX26^{f/f}$ P0-Cre-iCx26GJC showed drastically fragmented, small vesicle-like GJPs (Figures 6H, 6J, 6L, and 6N), as in the $CX26^{f/f}$ P0-Cre-cochlea (Figures 6B, 6D, and 6F).

As shown in Figure 6P, GJP lengths in $CX26^{f/f}$ P0-Cre-iCx26GJC (1.63 ± 0.07 μm) are significantly shorter ($p < 0.01$) than those of the WT (5.34 ± 0.28 μm), as in the cochlea (Figure 6O; WT, 4.72 ± 0.17 μm; $CX26^{f/f}$ P0-Cre, 1.76 ± 0.06 μm).

DISCUSSION

We report the development of a method to generate and proliferate iCx26GJCs from mouse iPSCs for use as a disease model and in inner-ear cell therapies targeting *GJB2*-related hearing loss, the most frequent type of hereditary deafness worldwide. Our induction method until day 7 was based on

previous studies (Koehler and Hashino, 2014; Koehler et al., 2013).

However, after the day-7 procedures, which screen for a CX26/CX30 highly expressing condition, isolation of CX26-positive small vesicles, and transferring CX26-positive small vesicles onto TRIC feeder cells, differ from previous studies (Koehler and Hashino, 2014; Koehler et al., 2013).

Previous studies have targeted the generation of inner-ear hair cell-like cells from ESCs/iPSCs (Chen et al., 2012; Koehler and Hashino, 2014; Koehler et al., 2013; Oshima et al., 2010). In contrast, we focused on CX26-GJP-forming cells derived from iPSCs, as the cochlear supporting cell-like cells. It has not been reported that ESCs/iPSCs differentiated into the cells with clear CX26-GJPs characterized by immunolabeling and gene expression for CX26/30, dye transfer assay, and Ca^{2+} imaging.

In the modified SFEBq method, we confirmed that the morphology and outer epithelium thickness of day 7–11 aggregates (Figure S2) were similar to those previously reported (Koehler et al., 2013). As these thin outer epithelia did not include the NANOG-GFP cells and were clearly demarcated, they could be separated by dissection for further adherent culture on cochlear feeder cells. In this process (Figure 1B), the medium conditions and the timing for optimal treatments were selected according to mRNA expression and gap junction formation as determined in subsequent experiments.

In the CX26 and CX30 mRNA expression analysis it has been suggested that the BMP- or the B/S-treatment condition is more suitable for differentiation into CX26- and CX30-expressing cells compared with the B/S + F/L treatment condition, which has been reported to differentiate into sensory epithelium (Koehler and Hashino, 2014; Koehler et al., 2013). It has also been suggested that the differentiation into neural ectoderm by SFEBq culture might be partially inhibited with respect to differentiation into non-neural ectoderm (Koehler and Hashino, 2014; Koehler et al., 2013), and the CX26/CX30 expression levels were increased by BMP supplementation with some regulation by additional supplements such as the transforming growth factor β (TGF-β) inhibitor, SB-431542 (Figure 1A). BMP signaling has been reported to be critical for induction of the non-neural ectoderm from the definitive ectoderm epithelium induced by SFEBq method (Eiraku and Sasai, 2012). TGF-β inhibitor (SB-431542) suppressed the undesirable induction of mesoderm induced by BMP signaling (Koehler and Hashino, 2014; Koehler et al., 2013).

The use of cochlear feeder cells was critical to the proliferation of the iCx26GJCs (Figure 2I) and the increase in CX26 plaque length (Figure 2J) in the dissected small vesicle of the aggregates. In contrast to the cochlear (TRIC) feeder system, a feeder system with chicken embryonic inner ear used for hair cell differentiation (Oshima et al., 2010) and feeder-free culture did not promote the cell proliferation or GJP formation of iCx26GJCs. Therefore, it is suggested that TRIC feeder cells may express some molecules to promote the proliferation and GJP formation of iCx26GJCs. Our working hypothesis is that a small number of cells that differentiated from iPSCs into CX26-expressing cells in modified SFEBq culture were induced to proliferate by the growth factors that were secreted from the cochlear feeder cells.

Our observation that iCx26GJCs co-expressed CX26 and CX30 (Figures 2K, 2L, and S4E–S4H) suggested that a number of cells in the aggregates had differentiated into cochlear non-sensory cells (Figures S4A–S4D) and generated CX26/CX30 GJPs; moreover, the data suggested that these cells had proliferated on the cochlear feeder cells after dissection of the small vesicles that were attached to the outer epithelium (Movie S2).

As a marker of cochlear supporting cells, we assessed $P27^{Kip1}$ localization in iCx26GJCs. $P27^{Kip1}$ is a cyclin-dependent kinase inhibitor that is thought to play a role in maintaining the postmitotic state of cochlear supporting cells such as the Deiters' cells and outer- and inner-sulcus cells. The $P27^{Kip1}$ signals were observed at the stage at which colony expansion (Movie S2) had almost stopped (~days 14–16). In the 2D cultures, we observed both heterogeneous (Figures 2M and S5C–S5E) and homogeneous (Figures S5F–S5I) $P27^{Kip1}$-positive regions including iCx26GJCs. This suggests that a portion of the iCx26GJCs gradually matures concomitantly with $P27^{Kip1}$ expression and that proliferation ceases when the cells stop expressing $P27^{Kip1}$ to maintain the postmitotic state, i.e., serving as cochlear supporting cells (Figures S5A and S5B). White et al. (2006) reported that isolated $P27^{kip1}$-positive mouse cochlear supporting cells retained the ability to divide when cultured with periotic mesenchymal cells, which support the growth and differentiation of cochlear sensory progenitors. In the present study, we also used inner-ear tissue-derived feeder cells for the differentiation and proliferation of iPS-derived cells, and we generated $CX26^{+}$/$P27^{Kip1+}$ supporting cell-like cells. These results suggest that cochlear feeder cells support the proliferation and further differentiation of iCx26GJCs.

We assessed SOX2 localization in iCx26GJCs and observed heterogeneous (Figures 2N and S6D–S6I) SOX2 expressions as in the adult mouse cochlea (Figures S6A–S6C). Mak et al. (2009) reported that the SOX2 signals were observed in the developing cochlear supporting cells, such as the Deiters' cells, Hensen cells, inner phalangeal cells, pillar cells, and part of inner-sulcus cells.

These results, whereby iCx26GJCs and mouse cochleae were stained with CX26, CX30, P27kip1, and SOX2 (Table

S1), suggested that iCx26GJCs are a cell type similar to the cochlear supporting cells.

TEM of iPSC-derived aggregates detected an ultrastructure typical of gap junctions (Figures 3A–3G). These characteristic structures were observed in the two medium conditions, BMP (Figures 3A–3E) and B/S (Figures 3F and 3G), but not in others (data not shown). These results suggest that the upregulated CX26 and CX30 proteins (Figure 1A) formed gap junctions within the iPSC aggregates. Prior to this study, little or no such ultrastructural formations typical of gap junctions had been reported as having been reproducibly induced from ESCs/iPSCs. Scanning EM of the cellular ultrastructure from 2D cultures at day 15 showed distinct straight cell borders that formed hexagonal or pentagonal shapes with associated microvilli dispersed along the borders (Figures 3J and 3K). This suggested that the differentiated iPSCs formed the surface structures typical of the inner and outer sulcus cells that surround cochlear hair cells (Figures 3H and 3I).

The scrape-loading assay of iCx26GJCs showed gradients and distance of dye transfers typical of those formed by functional GJIC networks (Figures 4C, 4F, and 4J) as previously reported (Yum et al., 2007, 2010). In contrast, such intercellular transfer of LY was not observed in undifferentiated iPSCs or TRIC used as feeder cells (Figures 4A, 4B, 4D, 4E, and 4J). These results suggest that CX26 and CX30 formed functional GJIC networks among iCx26GJCs, as is the case in cochlear tissue.

The Ca^{2+} imaging of 2D cultures revealed spontaneous Ca^{2+} transients and their propagation (Figures 5A, 5B, and 5D–5F; Movies S4 and S6), which is typical of the developing cochlea. As the spontaneous Ca^{2+} signaling activity was reversibly inhibited by a p2x receptor antagonist (PPADS: Figure 5C [middle] and Movie S5) and connexin hemichannel blocker (FFA: Figure 5C [bottom] and Movie S5), these results suggested that the Ca^{2+} activities required ATP and hemichannels, as has been reported for these activities in developing cochlea (Schutz et al., 2010; Tritsch et al., 2007).

Such spontaneous Ca^{2+} transients have been reported in postnatal mouse cochlear supporting cells (Tritsch et al., 2007), and the Ca^{2+} signals were suggested to be propagated via gap junctions and hemichannels containing CX26 and CX30 (Anselmi et al., 2008; Schutz et al., 2010). It was also suggested that such spontaneous Ca^{2+} signals in supporting cells may play a crucial role in generating the periodic, high-frequency burst of activity observed in the auditory center of the brain (Wang et al., 2015). Therefore, iCx26GJCs in the 2D cultures may differentiate into postnatal cochlear supporting cells before the onset of hearing.

In iCx26GJC from a CX26-deficient deafness mouse model ($CX26^{f/f}$ P0-Cre), GJP formations showed visible drastic disruption (Figures 6H, 6J, 6L, and 6N), reported to be a primary pathology of *GJB2*-related hearing loss (Kamiya et al., 2014). This suggests that the iPSCs derived from $CX26^{f/f}$ P0-Cre mouse have the potential to differentiate into iCx26GJC as an in vitro disease model of *GJB2*-related hearing loss. By using these cells, it is expected to establish the drug screening and inner-ear cell therapy after in vitro restoration of GJPs by the *GJB2* gene transfer (Iizuka et al., 2015) targeting *GJB2*-related hearing loss.

In summary, we hypothesize that iPS-derived cells formed floating aggregate in serum-free medium (SFEBq culture), after which the culture conditions including BMP (BMP4) and TGF-β inhibitor (SB-431542) treatment were selected to generate high-CX26/CX30 aggregates. Unlike hair cell differentiation (Koehler and Hashino, 2014; Koehler et al., 2013), these characteristic iPSC aggregates form distinct epithelia and small vesicles attached to the outer epithelium. In 2D culture, these small vesicles colonized on TRIC feeder cells. The small vesicle-derived colony exhibits proliferation potency and contains iCx26GJCs. The iCx26GJCs form functional CX26-GJPs that exhibit spontaneous ATP- and hemichannel-mediated Ca^{2+} transients typical of the developing cochlea. By using this method, we generated the in vitro disease model cells with GJP disruption for *GJB2*-related hearing loss (Figure 7).

In the present study, we demonstrated that the aggregate formation of iPSCs under several medium conditions followed by adherent culture with cochlear feeder cells induced: (1) the upregulation of mRNAs encoding CX26/CX30; (2) GJP formation composed of CX26/CX30; (3) the ultrastructure typical of gap junctions; (4) functional GJIC networks; and (5) spontaneous ATP- and hemichannel-mediated Ca^{2+} transients typical of developing cochlea. These are known to be the biological properties of cochlear supporting cells. Cochlear supporting cells are the most CX26-abundant cells that play crucial roles in maintaining proper endocochlear potential via ion transport. Furthermore, the disease model cells with *GJB2* mutation showing drastic GJP disruptions in the present study are thought to be the optimum therapeutic target for the treatment of *GJB2*-related hearing loss, the most typical type of hereditary deafness worldwide. It is expected, then, that these iPS-derived cells, which can be obtained from patients, will be particularly useful for drug screening and inner-ear cell therapies targeting *GJB2*-related hearing loss.

EXPERIMENTAL PROCEDURES

iPSC Lines and Maintenance Method

In the present study, we used five lines of mouse iPSCs. Two cell lines (cell names: iPS-MEF-Ng-178B-5 and iPS-MEF-FB/Ng-440A-3) were provided by RIKEN Bio Resource Center Cell Bank, and we generated three cell lines from murine embryonic

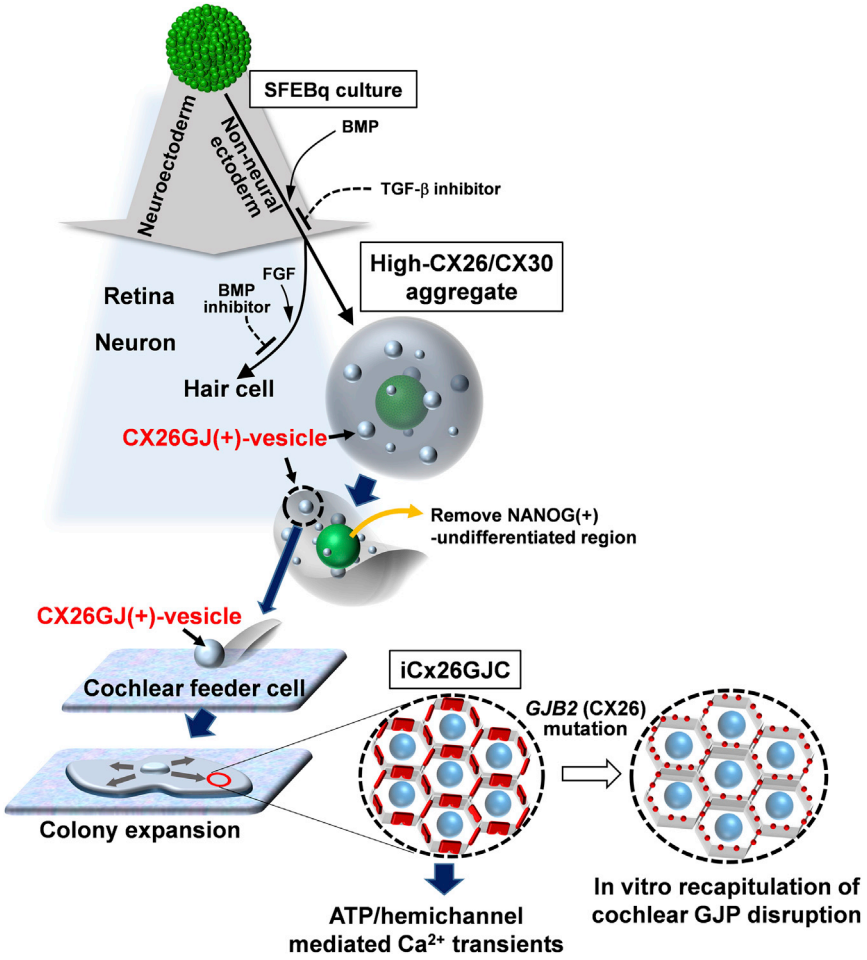

Figure 7. Schematic of In Vitro iPSC Differentiation into Functional iCx26GJCs and Disease Model Cells for *GJB2*-Related Hearing Loss

Undifferentiated iPSCs formed floating aggregate in serum-free medium (SFEBq culture). SFEBq culture generates neuroectoderm tissues such as retinal and neuronal tissues. Non-neural ectoderm such as inner-ear hair cell is also generated by this culture. The culture conditions including BMP (BMP4) and TGF-β inhibitor (SB-431542) treatment were selected to generate high-CX26/CX30 aggregates with high mRNA expressions. Unlike hair cell differentiation, these characteristic iPSC aggregates form distinct epithelia and small vesicles attached to the outer epithelium. After the removal of NANOG(+)-undifferentiated region, these small vesicles, which contain iCx26GJCs, are dissected and added onto cochlear feeder cells. They attach to the cochlear feeder cells (TRIC) and undergo colony expansion. The small vesicle-derived colony exhibits proliferation potency and contains iCx26GJCs. The iCx26GJCs form functional CX26-GJPs that exhibit spontaneous ATP- and hemichannel-mediated Ca^{2+} transients typical of the developing cochlea. In *GJB2* (CX26) mutant iPSCs, GJP disruption, which has been reported to be a primary pathology of *GJB2*-related hearing loss, is recapitulated in vitro.

fibroblasts (Oriental Yeast), murine cochlear fibroblasts derived from C57BL/6J mice, and fibroblasts derived from $CX26^{f/f}$ P0-Cre-mice that we have developed as a model for *GJB2*-related hearing loss (Kamiya et al., 2014) using Sendai virus vectors (Cytotune-iPS, DNAVEC). These five iPSC lines were maintained in feeder-free conditions.

All experimental protocols using mouse tissues were approved by the Institutional Animal Care and Use Committee at Juntendo University School of Medicine and were conducted in accordance with the US National Institutes of Health Guidelines for the Care and Use of Laboratory Animals.

iPSC Differentiation

Experiments covering days 0–11 of differentiation were performed as described previously (Koehler and Hashino, 2014; Koehler et al., 2013) with slight modifications. On day 3, BMP4 (10 ng/mL) and SB431542 (1 μM), either separately or together, were added at 5× concentration in 25 μL of fresh medium to the wells corresponding to BMP, SB, or BMP/SB, respectively. On day 4, FGF2 (25 ng/mL) and LDN193189 (1 μM), either separately or together, were added at 6× concentration in 25 μL of fresh medium to the wells corresponding to B/S + FGF, B/S + LDN, and F/L, respectively. On days 7–11, the regions with small vesicles transferred to inner-ear-derived feeder cells. TRICs were generated by overexposing cochlear tissue to trypsin and screening for the trypsin-resistant colonies. The adult (10-week-old mice) cochlear tissue used for the preparation of TRIC included the organ of Corti, basilar membrane, and lateral wall. They are mainly composed of supporting cells, hair cells, cochlear fibrocytes, and the other cells in the basilar membrane. This cell line was used as inner-ear-derived feeder cells to proliferate the otic progenitor cells. For the preparation of feeder cell layers, $3 \times 10^5/cm^2$ TRICs were seeded on gelatin-coated 24-well culture plates after mitomycin C (10 μg/ml) treatment for 3 hr.

qPCR

Total RNA was isolated using the RNeasy Plus Mini kit (Qiagen) and was reverse transcribed into cDNA using a PrimeScript II first-strand cDNA Synthesis kit (Takara). Real-time PCR was performed with the reverse transcription products, TaqMan Fast advanced master mix (Applied Biosystems), and gene-specific TaqMan Probe (Applied Biosystems) on a 7500 Fast Real-Time PCR system (Applied Biosystems). The Applied Biosystems 7500 Fast software was used to analyze the C_T values of different mRNAs normalized to an endogenous control (ACTB). TaqMan Probes (Assay ID; Applied Biosystems) were used to detect expression of mouse

GJB2 (Mm00433643_s1), *GJB6* (Mm00433661_s1), and *ACTB* (Mm02619580_g1).

Immunohistochemistry

The following primary antibodies were used: CX26 (mouse immunoglobulin G [IgG], 33-5800, Life Technologies), CX30 (rabbit IgG, 71-2200, Life Technologies), $P27^{kip1}$ (rabbit IgG, RB-9019-P0, *Neo* Markers), and SOX2 (goat IgG, sc-17320, Santa Cruz Biotechnology). The following secondary antibodies were used: Cy3-conjugated anti-mouse IgG, Alexa Fluor 488-conjugated anti-rabbit IgG, Alexa Fluor 488-conjugated anti-mouse IgG, Alexa Fluor 594-conjugated anti-goat IgG, and phalloidin TRITC.

Transmission Electron Microscopy

Aggregates were fixed with 2% paraformaldehyde and 2% glutaraldehyde in 0.1 M cacodylate buffer for 24 hr at 4°C and postfixed for 1.5 hr with 2% osmium tetroxide in phosphate buffer. Aggregates were dehydrated through a graded ethanol series and embedded in Epon. Aggregate sections were stained with uranyl acetate and lead citrate and examined by EM (Model H-7700, Hitachi).

Scanning Electron Microscopy

Aggregates, 2D cultures, and mouse cochleae were fixed with 2.5% glutaraldehyde in 0.1 M PBS for 24 hr at 4°C and postfixed with 2% osmium tetroxide in 0.1 M PBS for 2 hr. Samples were dehydrated in ethanol and freeze-dried with *tert*-butyl alcohol in a freeze dryer (ES-2030; Hitachi). After drying, samples were coated with osmium tetroxide and visualized with a scanning electron microscope (S-4800; Hitachi) at an accelerating voltage of 3.0 kV.

Dye Transfer with Scrape Loading

Dye transfer was investigated using a scrape-loading assay (Yum et al., 2007). iCx26GJC-containing proliferated cells were grown for 7–14 days after transfer onto TRIC feeder cells. The undifferentiated iPSCs and TRIC feeder cells were grown to confluency on coverslips as control. The medium was changed to Hank's balanced salt solution plus 0.1% LY (LY CH, Invitrogen). Many parallel lines were cut into the dish with a razor blade, and after 15 min cells scrape-loaded with LY were washed three times with Hank's balanced salt solution and imaged. Scrape loading was quantified by measuring the distance from the scrape line to the point where the fluorescence intensity dropped to 1.5× the background intensity. The images were processed and analyzed with NIH ImageJ software, and the mean distance was calculated using Microsoft Excel software.

Ca^{2+} Imaging and Pharmacological Study

The propagation of spontaneous Ca^{2+} transients via gap junctions in iCx26GJCs was carried out using methods modified from a previous study (Schutz et al., 2010). Samples were incubated for 20 min at 37°C in high-calcium Dulbecco's PBS (DPBS) containing 2 mM $CaCl_2$ (Nacalai Tesque) in DPBS (Gibco) supplemented with 5 μM fluo-4 AM (Dojindo), 0.01% (w/v) pluronic F-127 (Invitrogen), and 250 μM sulfinpyrazone (Sigma) as loading medium. To record spontaneous Ca^{2+} transients, we replaced the loading medium with low-calcium DPBS, which contained 20 μM $CaCl_2$.

The pharmacological study of iCx26GJCs was carried out using methods modified from previous studies (Schutz et al., 2010; Tritsch et al., 2007). The spontaneous Ca^{2+} activity was recorded for 3 min, then the cells were superfused with PPADS (50 μM; Tocris) or FFA (50 μM; Sigma) for 5 min, followed by washout of the drug and superfusion with low-Ca^{2+} DPBS for 8 min. Sequential fluorescence images were acquired using a Nipkow disc confocal system (CSU22, Yokogawa) and AQUACOSMOS software (Hamamatsu Photonics). Live-cell imaging experiments were performed at near-physiological temperature (32°–35°C) or room temperature (24°–26°C). Signals were measured as relative changes of fluorescence intensity ($\Delta f/f_0$), where f_0 is the minimum fluorescence and f is the recorded fluorescence, and $\Delta f = f - f_0$.

Statistical Analysis

Data were analyzed using Microsoft Excel software. Data are presented as mean ± SE. Statistical tests were performed using a two-tailed Student's t test with a significance criterion of $p < 0.05$ to compare relative mRNA levels, number of iCx26GJCs, and the GJP length. Scheffe's multiple comparison test, with a significance criterion of $p < 0.05$, was used to compare the distance of dye transfer.

SUPPLEMENTAL INFORMATION

Supplemental Information includes Supplemental Experimental Procedures, six figures, one table, and six movies and can be found with this article online at http://dx.doi.org/10.1016/j.stemcr.2016.10.005.

AUTHOR CONTRIBUTIONS

K.K. conceived and designed the experiments. I.F., A.F., K.H., T.A., A.N. and K.K. performed the experiments. N.K., T.N., O.M. and K.I. contributed reagents/materials/analysis tools. K.K. and I.F. wrote the paper.

ACKNOWLEDGMENTS

We thank M. Yoshida for help with transmission electron microscopy, K. Karasawa, K. Kobayashi, and Y. Furuta for experimental assistance, and T. Sakurai for help in the use of the facilities. This work was supported in part by JSPS KAKENHI grant number 25462653 (to K.K.), grant number 25293351 (to K.I.), and grant number 15K20229 (to I.F.), MEXT-support program for the Strategic Research Foundation at Private Universities, 2011–2015 (to K.I.), the Research on Intractable Diseases from Japan Agency for Medical Research and Development, AMED grant number 15ek0109125h0001 (to K.K.), Promotion and mutual aid corporation for Private Schools of Japan (to K.K.), the Terumo Life Science Foundation (to K.K.), and Takeda Science Foundation (to K.K.).

Received: August 2, 2016
Revised: October 12, 2016
Accepted: October 13, 2016
Published: November 10, 2016

REFERENCES

Ahmad, S., Chen, S., Sun, J., and Lin, X. (2003). Connexins 26 and 30 are co-assembled to form gap junctions in the cochlea of mice. Biochem. Biophys. Res. Commun. *307*, 362–368.

Anselmi, F., Hernandez, V.H., Crispino, G., Seydel, A., Ortolano, S., Roper, S.D., Kessaris, N., Richardson, W., Rickheit, G., Filippov, M.A., et al. (2008). ATP release through connexin hemichannels and gap junction transfer of second messengers propagate Ca^{2+} signals across the inner ear. Proc. Natl. Acad. Sci. USA *105*, 18770–18775.

Birkenhager, R., Lublinghoff, N., Prera, E., Schild, C., Aschendorff, A., and Arndt, S. (2010). Autosomal dominant prelingual hearing loss with palmoplantar keratoderma syndrome: variability in clinical expression from mutations of R75W and R75Q in the GJB2 gene. Am. J. Med. Genet. A. *152A*, 1798–1802.

Bruzzone, R., Barbe, M.T., Jakob, N.J., and Monyer, H. (2005). Pharmacological properties of homomeric and heteromeric pannexin hemichannels expressed in *Xenopus* oocytes. J. Neurochem. *92*, 1033–1043.

Chan, D.K., Schrijver, I., and Chang, K.W. (2010). Connexin-26-associated deafness: phenotypic variability and progression of hearing loss. Genet. Med. *12*, 174–181.

Chen, W., Jongkamonwiwat, N., Abbas, L., Eshtan, S.J., Johnson, S.L., Kuhn, S., Milo, M., Thurlow, J.K., Andrews, P.W., Marcotti, W., et al. (2012). Restoration of auditory evoked responses by human ES-cell-derived otic progenitors. Nature *490*, 278–282.

Eiraku, M., and Sasai, Y. (2012). Mouse embryonic stem cell culture for generation of three-dimensional retinal and cortical tissues. Nat. Protoc. *7*, 69–79.

Eiraku, M., Takata, N., Ishibashi, H., Kawada, M., Sakakura, E., Okuda, S., Sekiguchi, K., Adachi, T., and Sasai, Y. (2011). Self-organizing optic-cup morphogenesis in three-dimensional culture. Nature *472*, 51–56.

Eskandari, S., Zampighi, G.A., Leung, D.W., Wright, E.M., and Loo, D.D. (2002). Inhibition of gap junction hemichannels by chloride channel blockers. J. Membr. Biol. *185*, 93–102.

Gomes, P., Srinivas, S.P., Van Driessche, W., Vereecke, J., and Himpens, B. (2005). ATP release through connexin hemichannels in corneal endothelial cells. Invest. Ophthalmol. Vis. Sci. *46*, 1208–1218.

Iizuka, T., Kamiya, K., Gotoh, S., Sugitani, Y., Suzuki, M., Noda, T., Minowa, O., and Ikeda, K. (2015). Perinatal Gjb2 gene transfer rescues hearing in a mouse model of hereditary deafness. Hum. Mol. Genet. *24*, 3651–3661.

Inoshita, A., Iizuka, T., Okamura, H.O., Minekawa, A., Kojima, K., Furukawa, M., Kusunoki, T., and Ikeda, K. (2008). Postnatal development of the organ of Corti in dominant-negative Gjb2 transgenic mice. Neuroscience *156*, 1039–1047.

Kamiya, K., Fujinami, Y., Hoya, N., Okamoto, Y., Kouike, H., Komatsuzaki, R., Kusano, R., Nakagawa, S., Satoh, H., Fujii, M., and Matsunaga, T. (2007). Mesenchymal stem cell transplantation accelerates hearing recovery through the repair of injured cochlear fibrocytes. Am. J. Pathol. *171*, 214–226.

Kamiya, K., Yum, S.W., Kurebayashi, N., Muraki, M., Ogawa, K., Karasawa, K., Miwa, A., Guo, X., Gotoh, S., Sugitani, Y., et al. (2014). Assembly of the cochlear gap junction macromolecular complex requires connexin 26. J. Clin. Invest. *124*, 1598–1607.

Kikuchi, T., Kimura, R.S., Paul, D.L., Takasaka, T., and Adams, J.C. (2000). Gap junction systems in the mammalian cochlea. Brain Res. Brain Res. Rev. *32*, 163–166.

Koehler, K.R., and Hashino, E. (2014). 3D mouse embryonic stem cell culture for generating inner ear organoids. Nat. Protoc. *9*, 1229–1244.

Koehler, K.R., Mikosz, A.M., Molosh, A.I., Patel, D., and Hashino, E. (2013). Generation of inner ear sensory epithelia from pluripotent stem cells in 3D culture. Nature *500*, 217–221.

Locher, H., Frijns, J.H., van Iperen, L., de Groot, J.C., Huisman, M.A., and Chuva de Sousa Lopes, S.M. (2013). Neurosensory development and cell fate determination in the human cochlea. Neural Dev. *8*, 20.

Locher, H., de Groot, J.C., van Iperen, L., Huisman, M.A., Frijns, J.H., and Chuva de Sousa Lopes, S.M. (2014). Distribution and development of peripheral glial cells in the human fetal cochlea. PLoS One *9*, e88066.

Locher, H., de Groot, J.C., van Iperen, L., Huisman, M.A., Frijns, J.H., and Chuva de Sousa Lopes, S.M. (2015). Development of the stria vascularis and potassium regulation in the human fetal cochlea: insights into hereditary sensorineural hearing loss. Dev. Neurobiol. *75*, 1219–1240.

Mak, A.C., Szeto, I.Y., Fritzsch, B., and Cheah, K.S. (2009). Differential and overlapping expression pattern of SOX2 and SOX9 in inner ear development. Gene Expr. Patterns *9*, 444–453.

Mauritz, C., Schwanke, K., Reppel, M., Neef, S., Katsirntaki, K., Maier, L.S., Nguemo, F., Menke, S., Haustein, M., Hescheler, J., et al. (2008). Generation of functional murine cardiac myocytes from induced pluripotent stem cells. Circulation *118*, 507–517.

Morton, N.E. (1991). Genetic epidemiology of hearing impairment. Ann. N. Y Acad. Sci. *630*, 16–31.

Morton, C.C., and Nance, W.E. (2006). Newborn hearing screening—a silent revolution. N. Engl. J. Med. *354*, 2151–2164.

Oshima, K., Shin, K., Diensthuber, M., Peng, A.W., Ricci, A.J., and Heller, S. (2010). Mechanosensitive hair cell-like cells from embryonic and induced pluripotent stem cells. Cell *141*, 704–716.

Oyamada, Y., Komatsu, K., Kimura, H., Mori, M., and Oyamada, M. (1996). Differential regulation of gap junction protein (connexin) genes during cardiomyocytic differentiation of mouse embryonic stem cells in vitro. Exp. Cell Res. *229*, 318–326.

Oyamada, M., Takebe, K., Endo, A., Hara, S., and Oyamada, Y. (2013). Connexin expression and gap-junctional intercellular communication in ES cells and iPS cells. Front. Pharmacol. *4*, 85.

Petersen, M.B., and Willems, P.J. (2006). Non-syndromic, autosomal-recessive deafness. Clin. Genet. *69*, 371–392.

Schutz, M., Scimemi, P., Majumder, P., De Siati, R.D., Crispino, G., Rodriguez, L., Bortolozzi, M., Santarelli, R., Seydel, A., Sonntag, S., et al. (2010). The human deafness-associated connexin 30 T5M mutation causes mild hearing loss and reduces biochemical coupling among cochlear non-sensory cells in knock-in mice. Hum. Mol. Genet. *19*, 4759–4773.

Stout, C.E., Costantin, J.L., Naus, C.C., and Charles, A.C. (2002). Intercellular calcium signaling in astrocytes via ATP release through connexin hemichannels. J. Biol. Chem. *277*, 10482–10488.

Sun, J., Ahmad, S., Chen, S., Tang, W., Zhang, Y., Chen, P., and Lin, X. (2005). Cochlear gap junctions coassembled from Cx26 and 30 show faster intercellular Ca2+ signaling than homomeric counterparts. Am. J. Physiol. Cell Physiol. *288*, C613–C623.

Takahashi, K., and Yamanaka, S. (2006). Induction of pluripotent stem cells from mouse embryonic and adult fibroblast cultures by defined factors. Cell *126*, 663–676.

Tritsch, N.X., Yi, E., Gale, J.E., Glowatzki, E., and Bergles, D.E. (2007). The origin of spontaneous activity in the developing auditory system. Nature *450*, 50–55.

Wang, H.C., Lin, C.C., Cheung, R., Zhang-Hooks, Y., Agarwal, A., Ellis-Davies, G., Rock, J., and Bergles, D.E. (2015). Spontaneous activity of cochlear hair cells triggered by fluid secretion mechanism in adjacent support cells. Cell *163*, 1348–1359.

White, P.M., Doetzlhofer, A., Lee, Y.S., Groves, A.K., and Segil, N. (2006). Mammalian cochlear supporting cells can divide and trans-differentiate into hair cells. Nature *441*, 984–987.

Yum, S.W., Zhang, J., Valiunas, V., Kanaporis, G., Brink, P.R., White, T.W., and Scherer, S.S. (2007). Human connexin26 and connexin30 form functional heteromeric and heterotypic channels. Am. J. Physiol. Cell Physiol. *293*, C1032–C1048.

Yum, S.W., Zhang, J., and Scherer, S.S. (2010). Dominant connexin26 mutants associated with human hearing loss have trans-dominant effects on connexin30. Neurobiol. Dis. *38*, 226–236.

Zhang, Y., McBride, D.W., Jr., and Hamill, O.P. (1998). The ion selectivity of a membrane conductance inactivated by extracellular calcium in *Xenopus* oocytes. J. Physiol. *508*, 763–776.